INSTITUTE OF COMPUTER SCIENCES
Master in Artificial Intelligence and Data Science

Universitätsstr. 1 D–40225 Düsseldorf

Heinrich Heine Universität Düsseldorf

AI-based fluorescent labeling for cell line development

Hanna Pankova

Master thesis

Date of issue: 01. April 2022
Date of submission: 29. August 2022
Reviewers: Prof. Dr. Markus Kollmann
Dr. Wolfgang Halter

Erklärung

Hiermit versichere ich, dass ich diese Master thesis selbstständig verfasst habe. Ich habe dazu keine anderen als die angegebenen Quellen und Hilfsmittel verwendet.

Düsseldorf, den 29. August 2022

Hanna Pankova

Abstract

Cell line development is an expensive and time-consuming process, however that is the most modern approach for producing the proteins needed in pharmaceuticals.

Contents

1 Introduction

1.1 Motivation

1.2 Notation

2 Domain knowledge

2.1 Biology

2.1.1 Cell line development process

General theory behind the cell line development process. Starting from what proteins are. How cells are developed. Difficulties of the cell line development process and timelines.

2.1.2 Project specifications of cell line development for Merck KgaA

Description of my project, why is it useful, what are the processes here. How my neural network can be used for further stability predictions.

2.2 Deep learning and machine learning basics

Introduction of the notaiton for the dataset, parameters, predictions.

2.2.1 Neural networks

Convolutional neural network, Autoencoder, embedding, optimizers, regularization, descriptions of how each layer works.

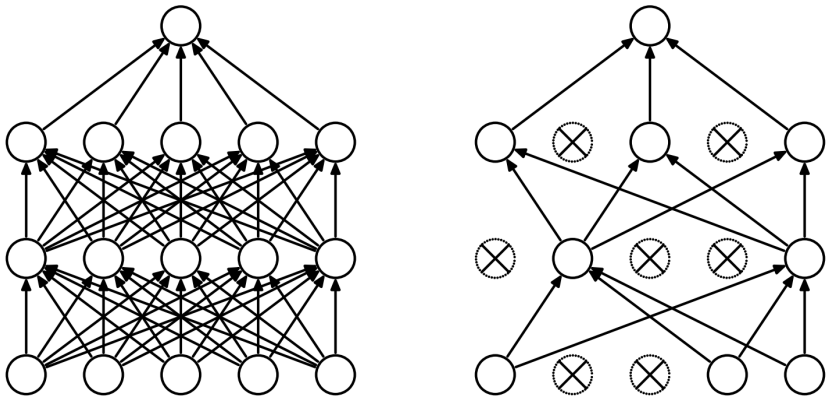

(a) Standard Neural Net (b) After applying dropout.

Figure 1: Dropout

2.2.2 Clustering

Theory of clustering algorithms, DBSCAN, HDBSCAN, PCA

2.3 Imaging

2.3.1 Digital imaging

How image is stored in memory, which conventions there are (RGB, BGR (conventions are used in corruptions augmentations)).

2.3.2 Microscopy imaging

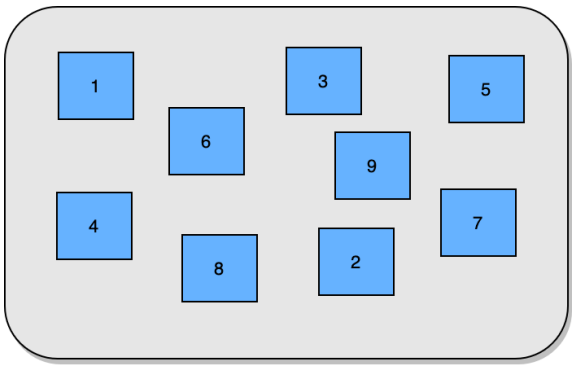

Figure 2: Way in which photos of the well-plate were taken

Which difficulties it may cause (validation loss is lower than train loss)

3 Model training

3.1 Neural network architecture

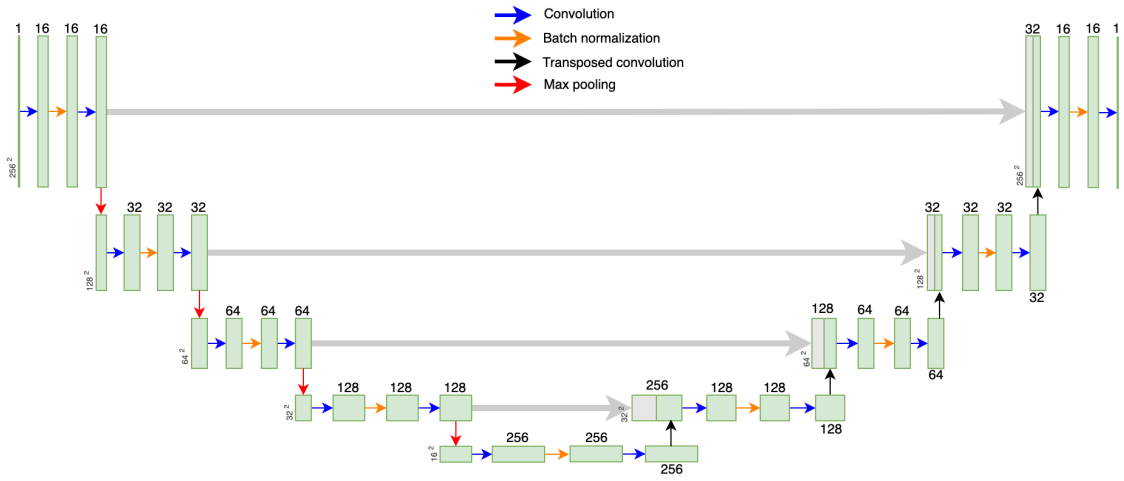

Figure 3: Unet

And information on the embeddings, output sizes, amount of parameters, etc.

3.2 Loss functions

Which loss functions were used, Pearson correlation coefficient explained.

3.3 Available data

Description of the datasets and the amount of images in each category.

Table 1: Available data for each fo the organelles

	Total images	Training crops	Validation crops	Test crops
Nuclei	595	27,264	3,008	7,616
Actin	400	18,432	2,048	5120
Golgi	761	23,036	2,336	6,347
H19	400	?	?	?
Nucleolei	?	?	?	?

3.4 Training costs estimation

Table with the estimation of costs and times for AWS

3.5 Augmentations

Description of all augmentations used

3.5.1 Smart augmentations for rotation and scaling

3.6 Convergence

Images of train and validation loss.

3.7 Model setup

3.7.1 Weight Initialization

These plots represent MSE

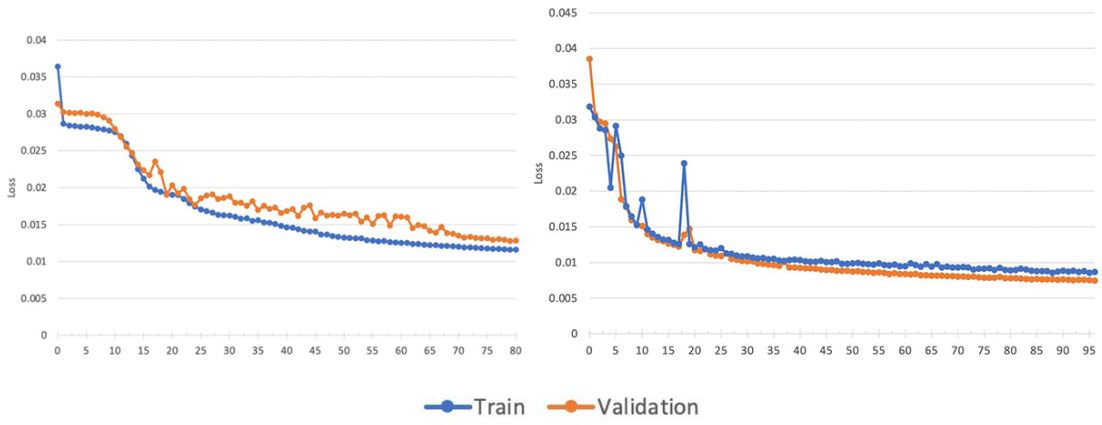

Figure 4: Nuclei training without and with custom weight initialization

3.7.2 Regularization

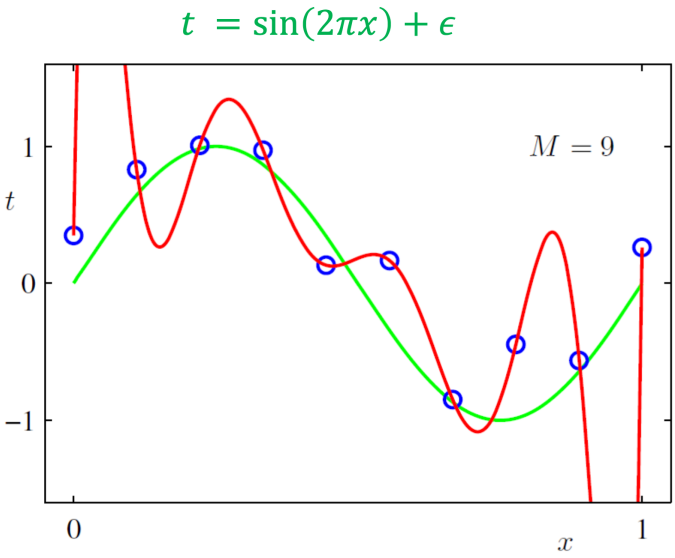

Figure 5: Overfitting

3.7.3 Optimizers

Comparison of different optimizers

4 Nuclei

4.1 Preprocessing

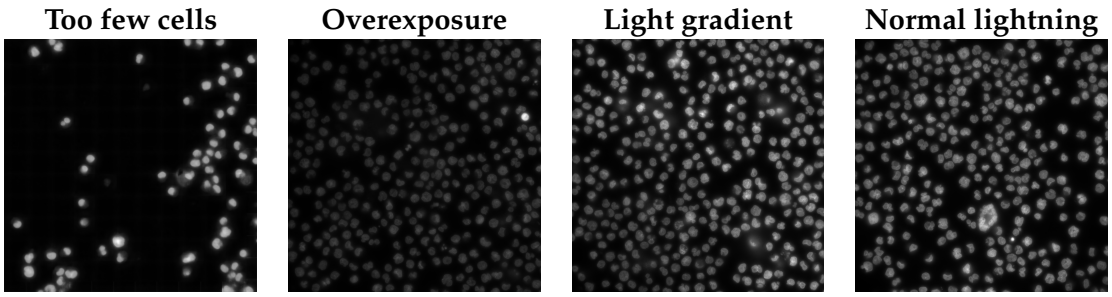

Figure 6: Different lightning conditions

4.1.1 Thresholding algorithms

Global and local thresholding

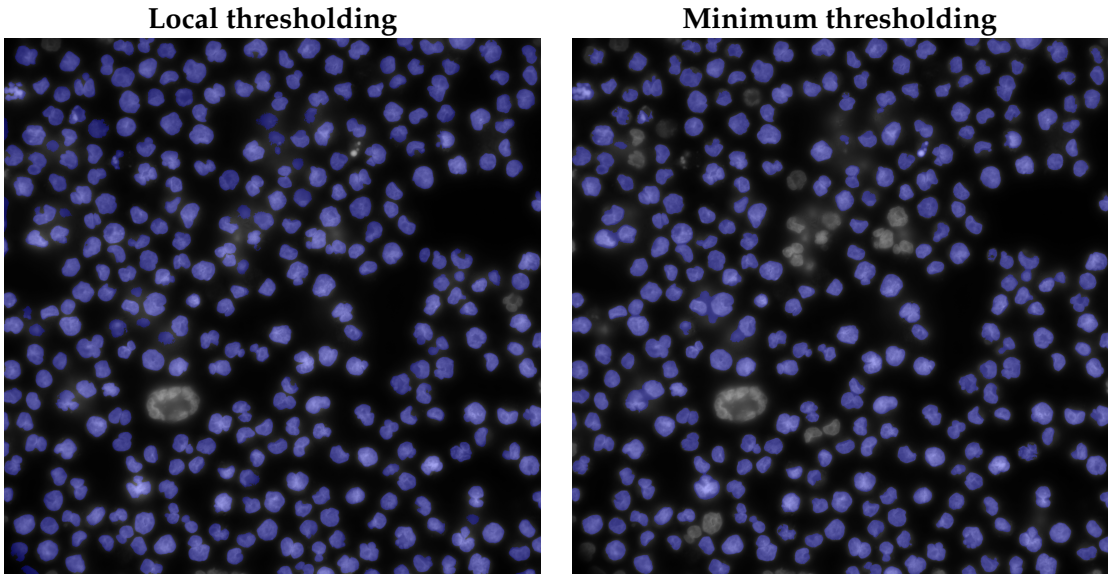

Figure 8: Local vs. Global thresholding (normal conditions)

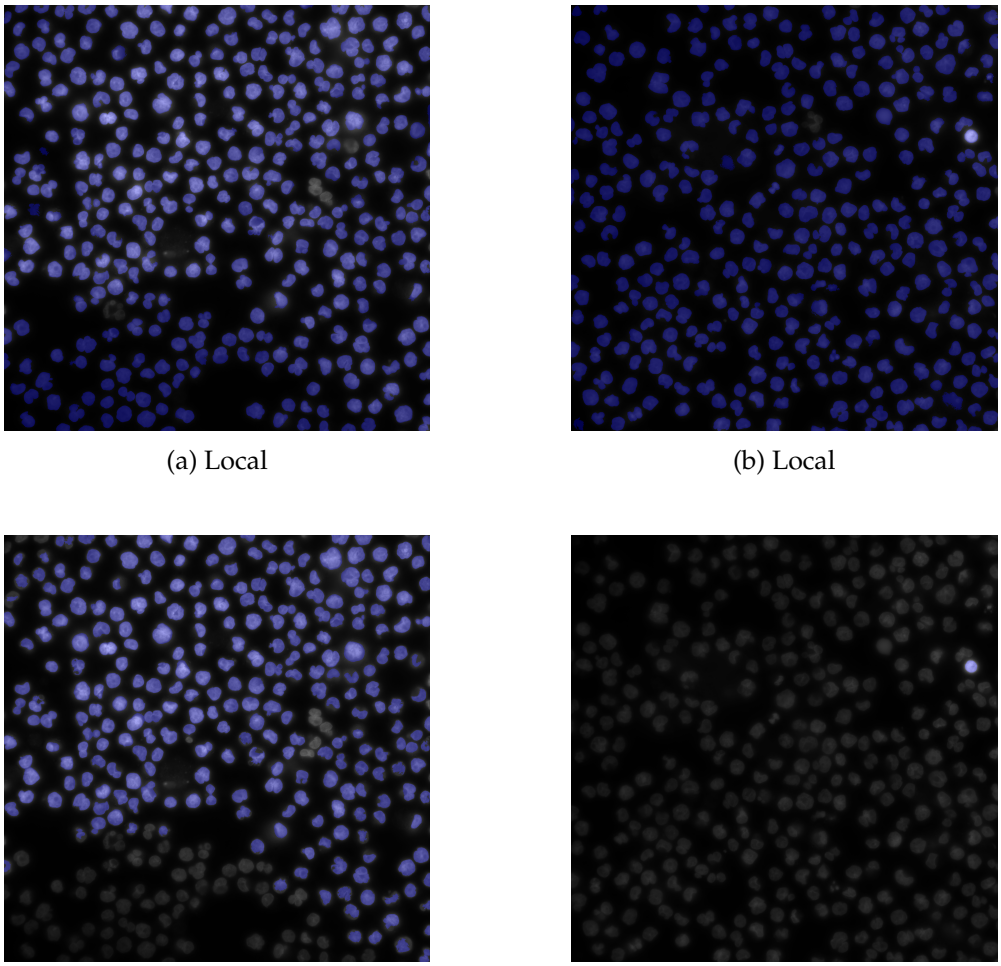

(a) Local (b) Local

(c) Global, minimum (d) Global, minimum

Figure 7: Local vs. Global thresholding

4.2 Training and predictions

4.2.1 Convergence

Has the model converged or not. Will more data help?

Not regularized yet, full dataset training with PCC

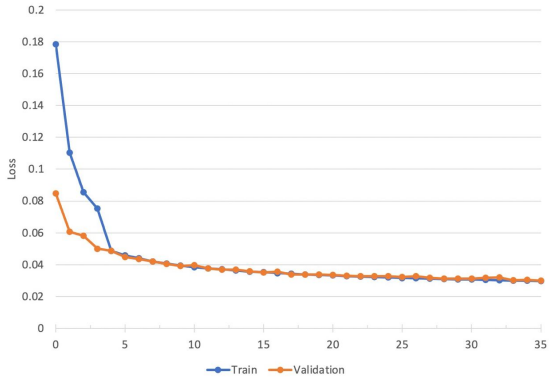

Figure 9: Having more data makes training more stable

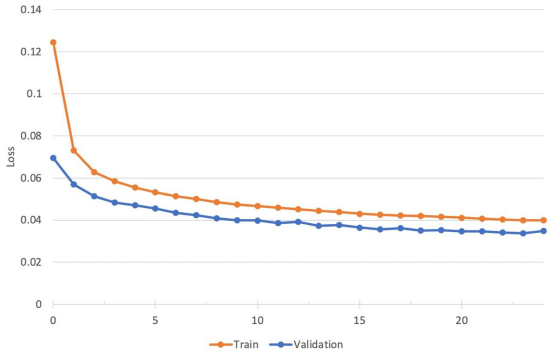

Figure 10: With regularization and augmentations PCC

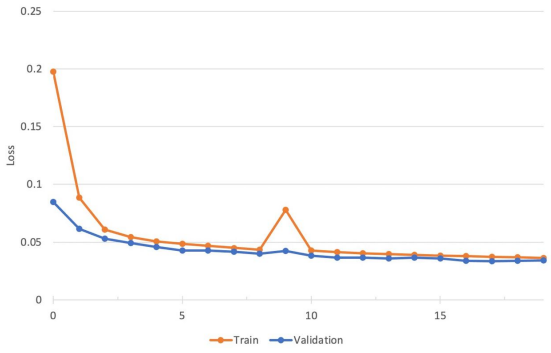

Figure 11: No regularization but augmentations

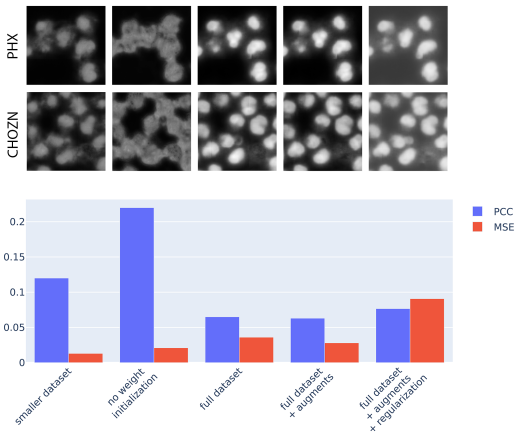

Figure 12: Difefrent models predictions and scores comparison

4.2.2 Predictions quality

Blurry, boundaries, not enough of details and possible improvements

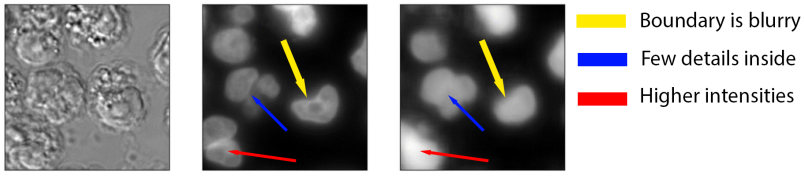

Figure 13: Some troubles in predictions

4.3 Postprocessing for nuclei segmentation

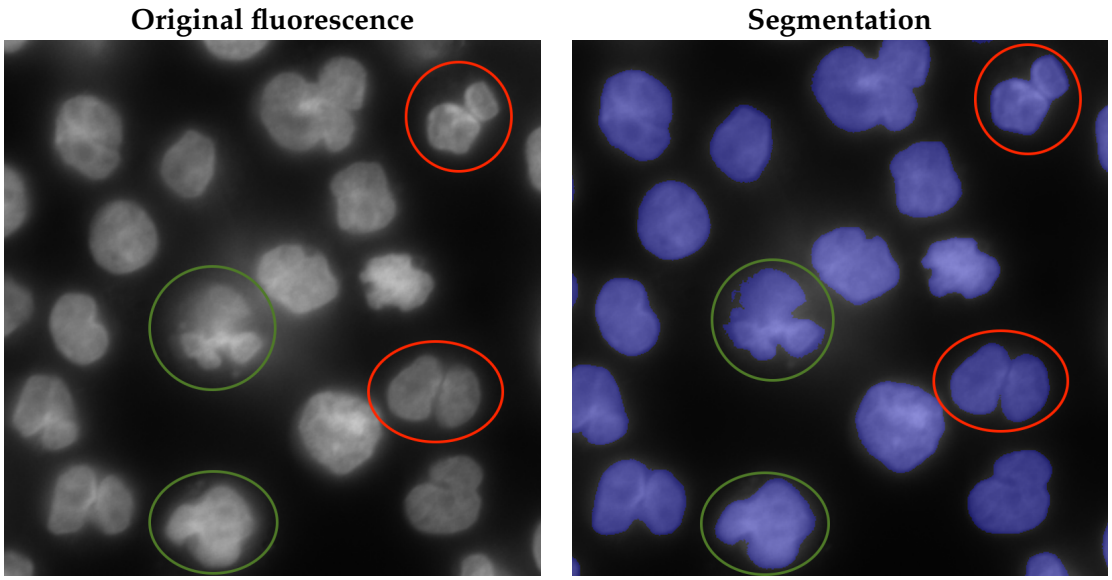

Figure 14: Closely located cells

Overall algorithm

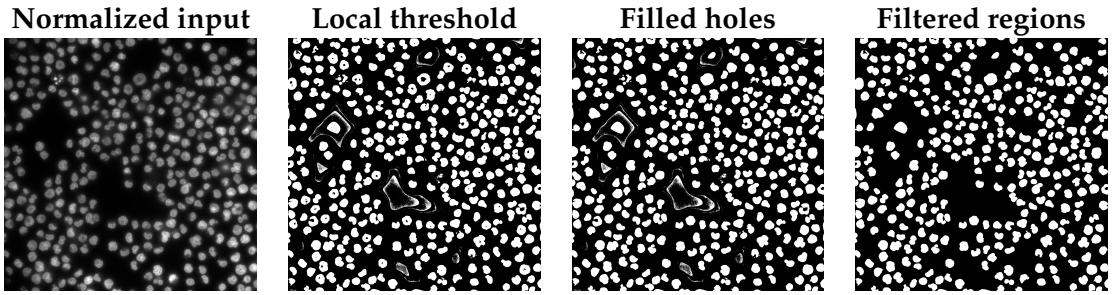

Figure 15: Fluorescence segmentation

4.4 Influence of scaling on predictions quality

Examples of predictions quality with different scales.

5 ER

5.1 Preprocessing

Algorithm 1 Fluorescence segmentation

1. Normalize image
2. Apply global *threshold_mean* to receive initial mask.
3. Zero out pixels outside the mask
4. Apply local thresholding.
5. Apply *fill_holes* transformation.
6. Morphological opening from opencv and Gaussian blur.
7. Run *findContours* from opencv in order to obtain separate regions and filter out too small regions.

Segmentation steps are also illustrated in Figure

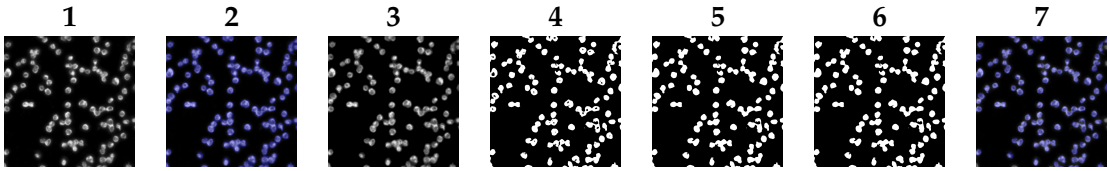

Figure 16: ER prediction

5.2 Training and predictions

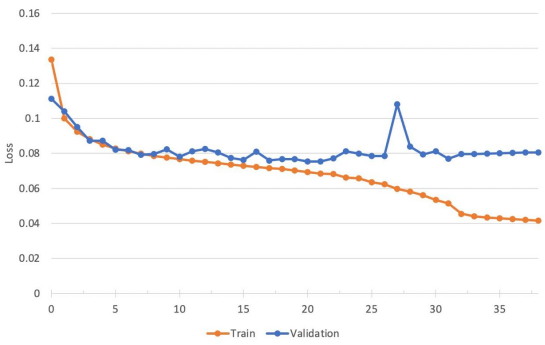

Figure 17: Overfit

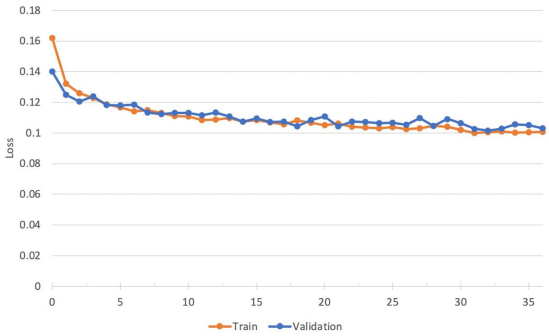

Figure 18: No overfit with augmentations

5.3 Postprocessing

5.4 Combination of nuclei and actin predictions

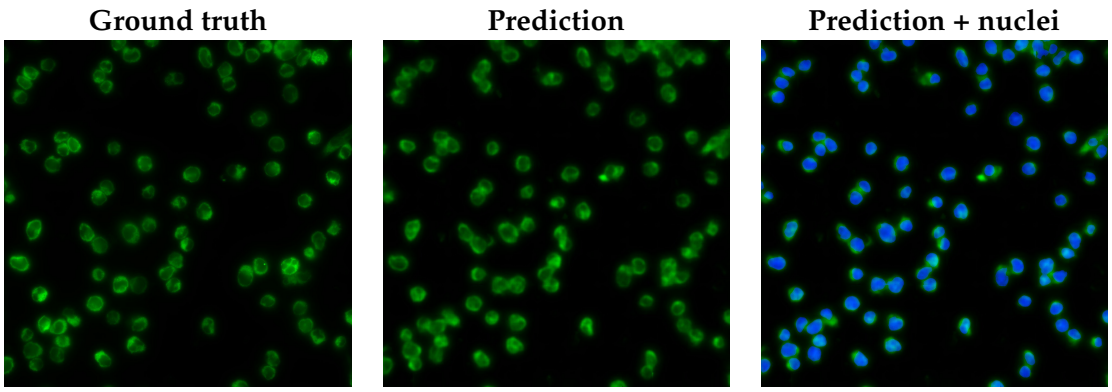

Figure 19: ER prediction

5.5 Prediction quality on the crop's border

5.6 Generalizability across phenotypes

6 Golgi

6.1 Preprocessing

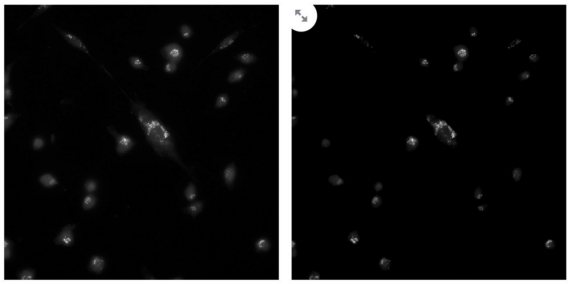

Figure 20: Golgi enhancement

6.1.1 Background removal algorithms

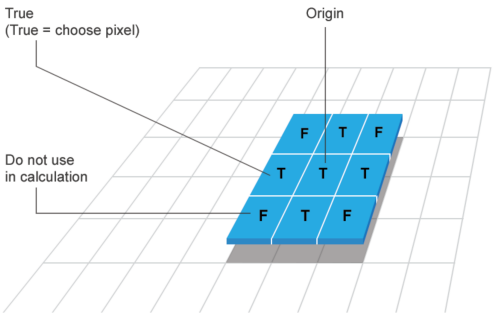

Figure 21: Structuring Element

Rolling ball algorithms

Rolling ball still leaves some noise

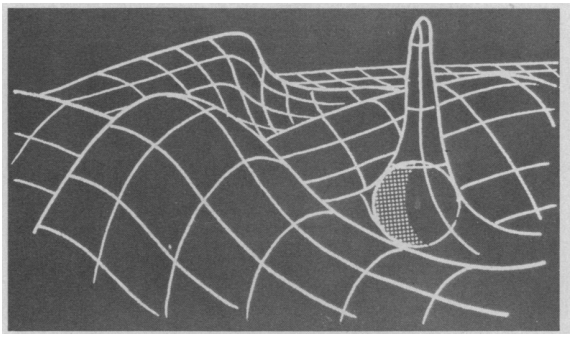

Figure 22: Rolling Ball

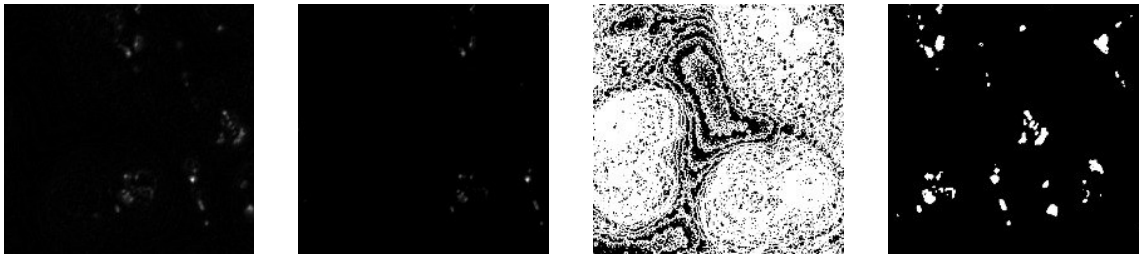

(a) (b) (c) (d)

Figure 23: (a) Vanilla pre-processing with automatic background removal algorithm only; (b) Additional clipping of lower intensities after vanilla pre-processing; (c) masked or subfigure (a); (d) mask of subfigure (b)

6.2 Training and predictions

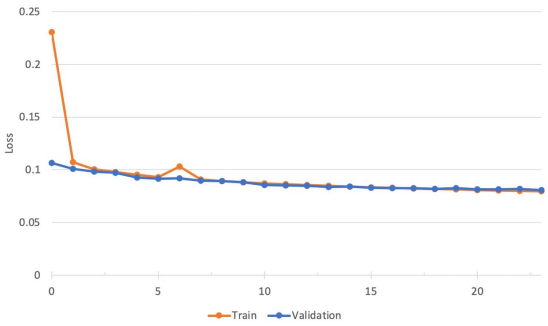

Figure 24: Straightforward training doesn't work

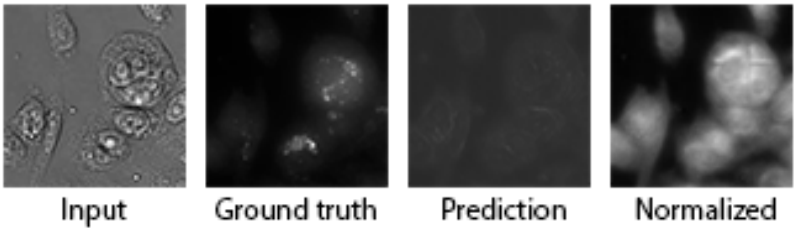

Figure 25: Training on original data

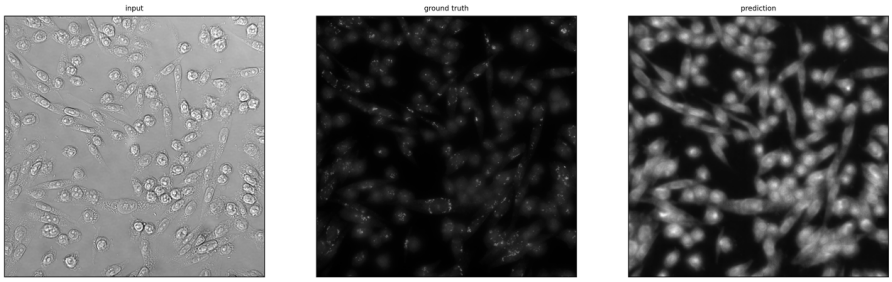

Figure 26: Full size predictions

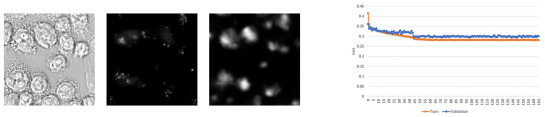

Figure 27: Training on the enhanced data

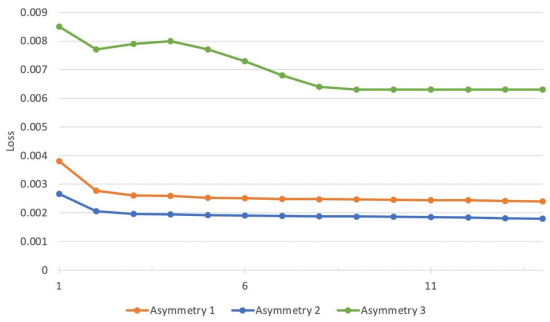

Figure 28: Asymmetrical training

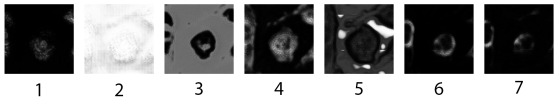

Figure 29: Asymmetrical training predictions

6.3 Alternative ways to improve predictions

6.3.1 Noise reduction methods

6.3.2 Asymmetrical losses

6.3.3 Use of gradient in loss

7 GFP prediction

7.1 Preprocessing

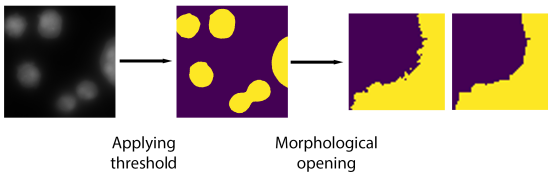

Figure 30: Converting gfp to a binary mask

7.2 Predictions

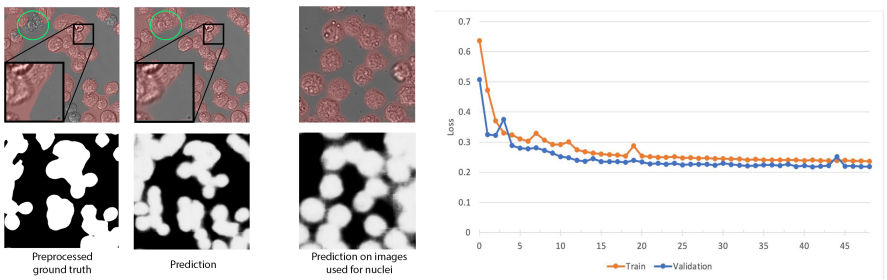

Figure 31: Binary training with BCE

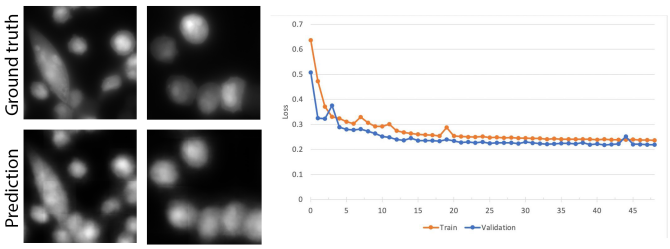

Figure 32: Training with Pearson correlation loss

Table 2: Correlation coefficients for downstream tasks

Binary training	Pearson	Spearman
Number of ER	0.67	0.64
Area	0.82	0.75
Continuos training	Pearson	Spearman
Number of ER	0.57	0.55
Area	0.26	0.64

7.3 Postprocessing

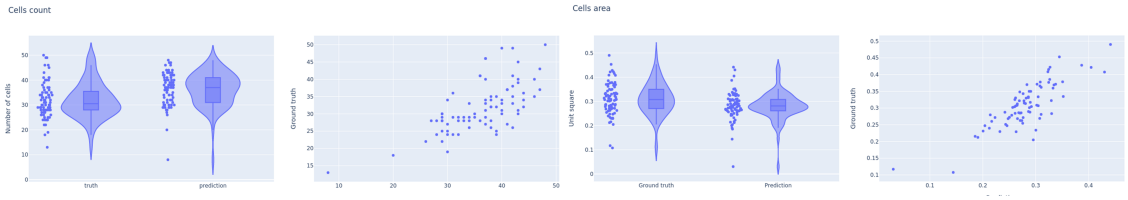

Figure 33: Downstream metrics

7.4 Combination of GFP, nuclei and ER

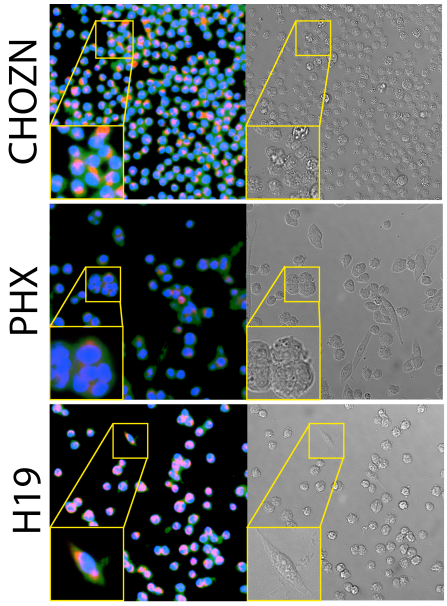

Figure 34: GFP, Nuclei and ER combined

8 Model Evaluation

8.1 Crops combination technique

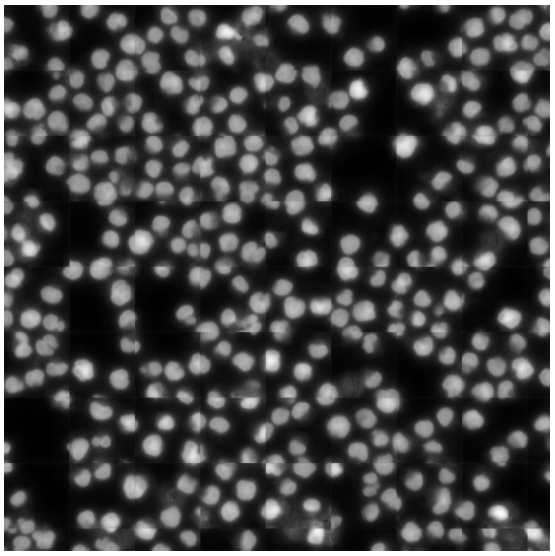

Figure 35: No overlap

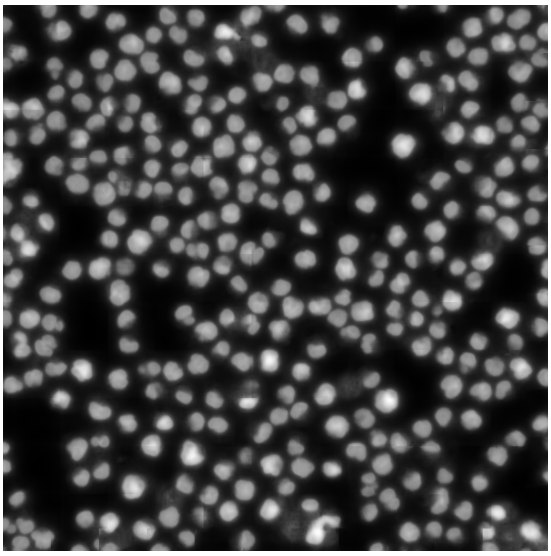

Figure 36: 30 pixels overlap

Improve this plot by showing the visible border explicitly, example of how it can influence a further segmentation perhaps?

8.2 Metrics for downstream tasks

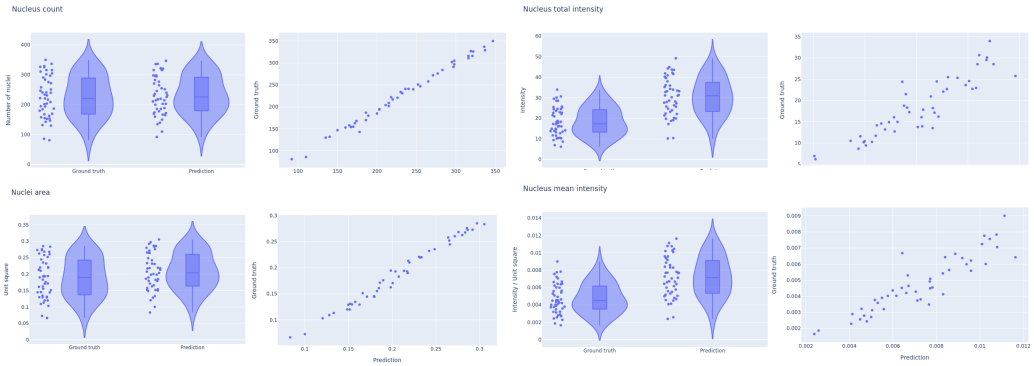

Figure 37: Metrics for downstream tasks on nuclei

Table 3: Correlation coefficients for downstream tasks

	Pearson	Spearman
Number of nuclei	0.995	0.994
Total intensity	0.902	.911
Mean intensity	0.907	0.904
Area	0.992	0.990

8.3 Influence of different loss functions on metrics for downstream tasks

9 Stability

9.1 Artificial corruptions

Description of artificial corruptions.

Table 4: Hyperparameter for different artificial corruption severities

Corruption \ Severity	-5	-4	-3	-2	-1	0	1	2	3	4	5
Defocus blur (radius)						0	0.5	1.0	1.5	2	3
Contrast (gain)	3.5	3.0	2.5	2.0	1.5	1	0.9	0.8	0.7	0.5	0.3
Brightness (bias)	-150	-135	-120	-90	-50	0	50	90	120	135	150

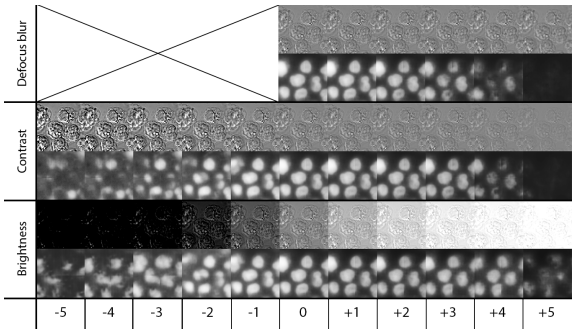

Figure 38: Influence of artificial corruptions on the predictions

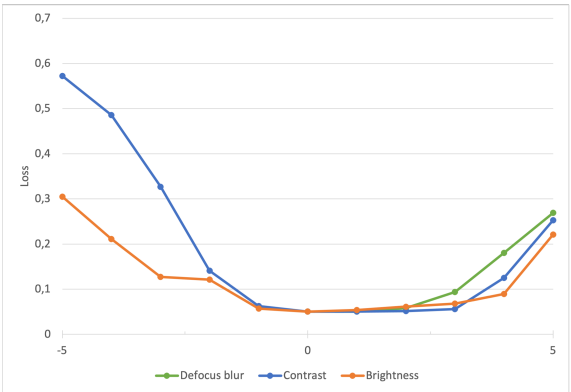

Figure 39: Change of loss for artificial corruptions

9.2 Real corruptions

9.3 Influence of corruptions on metrics for downstream tasks

9.4 Improving predictions with additional corruption augmentations

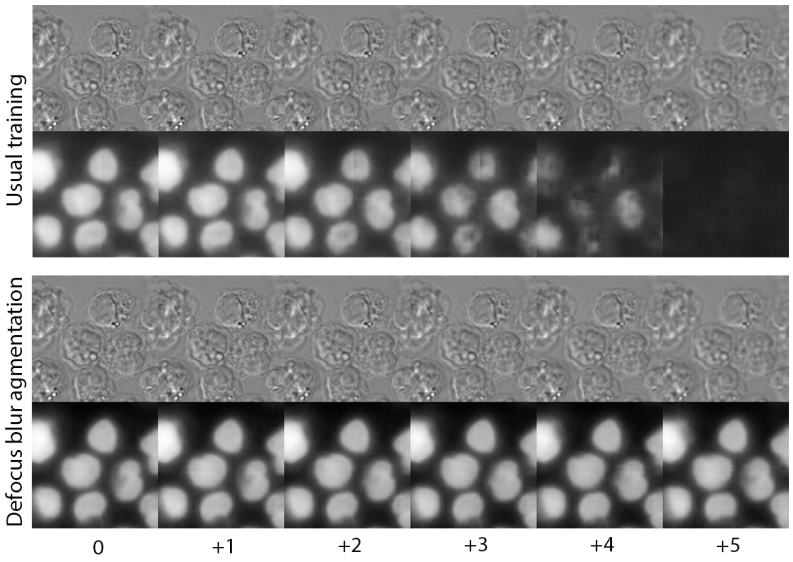

Figure 40: Using corruptions as augmentations improves predictions

10 Information in the UNET embeddings

10.1 Dimensionality reduction methods

10.2 UMAP, t-SNE, PCA

10.3 Autoencoder embeddings as an alternative

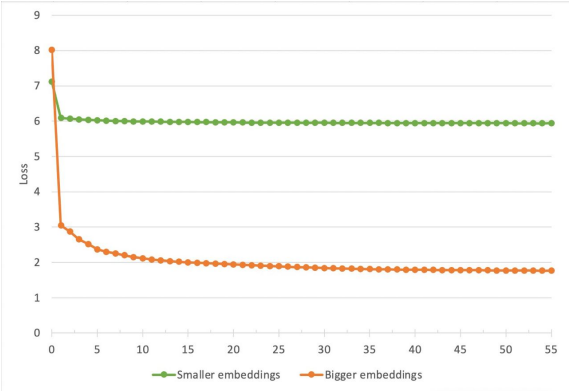

Figure 41: Autoencoders training convergence

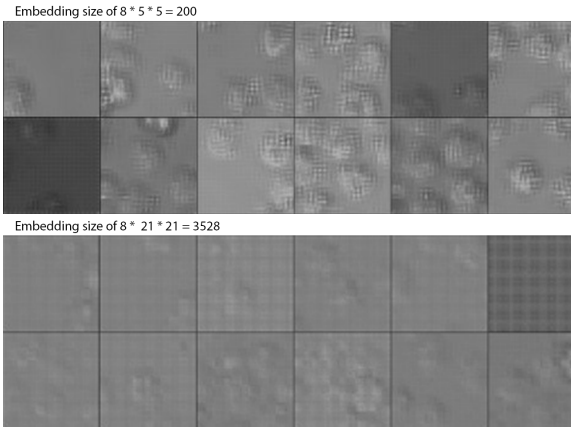

Figure 42: Samples drawn from the trained autoencoder

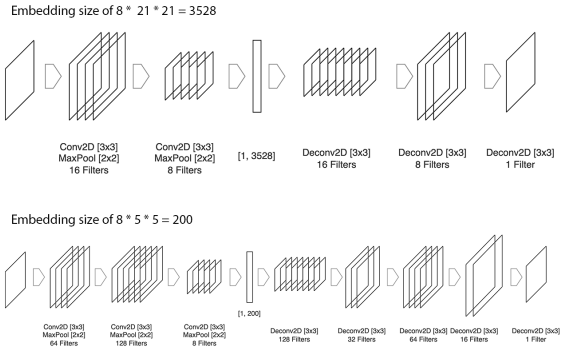

Figure 43: Architectures of two autoencoders

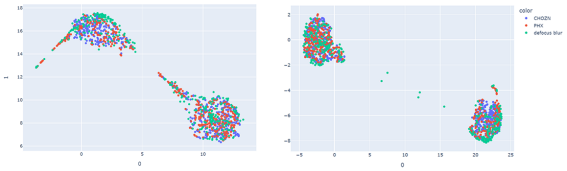

Figure 44: Autoencoder embeddings after applying PCA with 10 components and UMAP afterwards. Earlier epoch VS later epoch

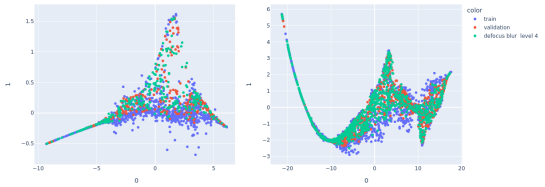

Figure 45: PacMAP does not provide information on the coruption

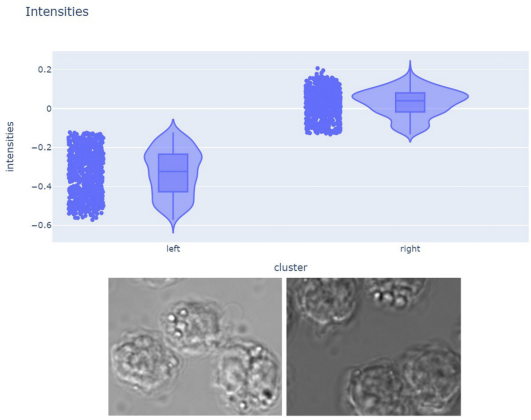

Figure 46: What do two UMAP clusters represent

10.4 Clustering

10.4.1 Clustering methods (HDBSCAN, DBSCAN, K-means)

10.4.2 Clustering on UNet embeddings

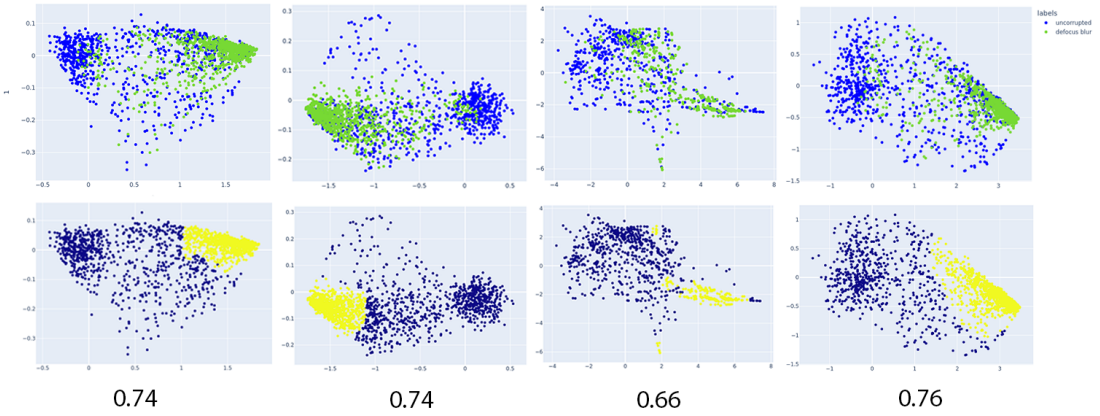

Figure 47: Clustering of UNet Embeddings

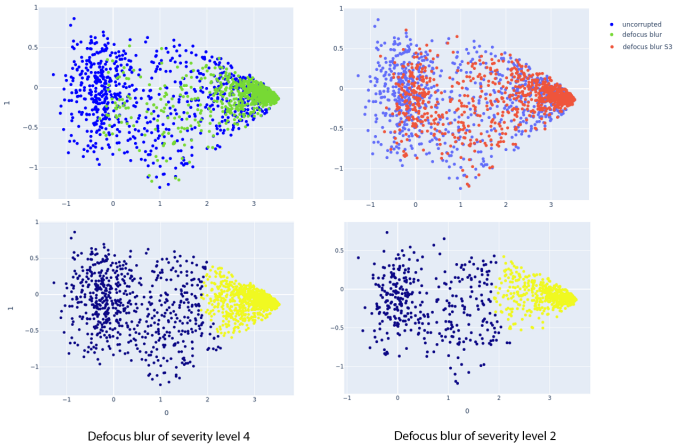

Figure 48: Clustering for different severities levels

TABLE with F1-score: 0.76 VS 0.64

11 Drift detection

11.1 A need to detect drift

11.2 MMD

11.2.1 Drift detection

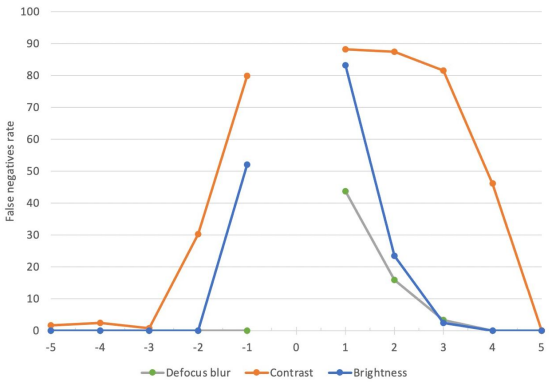

Figure 49: False negatives rate for drift detection on artificial corruptions

11.2.2 Online drift detection

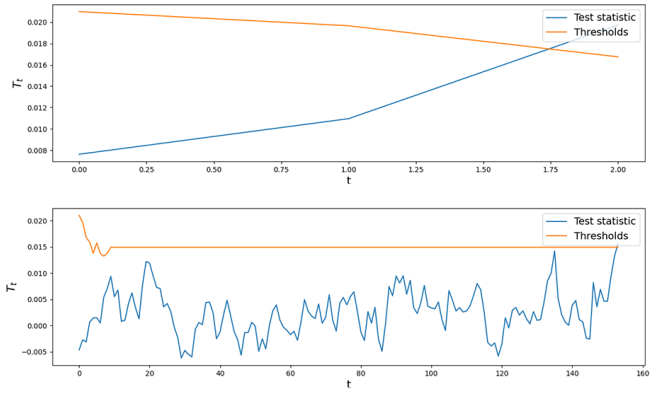

Figure 50: Expected runtime (ERT) for corrupted and in-distribution data

Table 5: Test window size influence on separability

W	2	5	10	15	20
Auc-Roc	0.85	0.92	0.98	0.90	0.88

Table 6: ERT influence on separability

W	32	64	128	256
Auc-Roc	0.90	0.95	0.98	0.98

Table 7: Severity of corruptions on separability

W	Level 2	Level 3	Level 4
Auc-Roc	0.84	0.92	0.98

Figure 51: AUC ROC scores for various defocus corruptions severities

12 Software Tools

12.1 Foundry. Palantir

12.2 AWS

12.3 Streamlit

12.4 ImageJ, CellProfiler

13 Summary

List of Figures

List of Tables